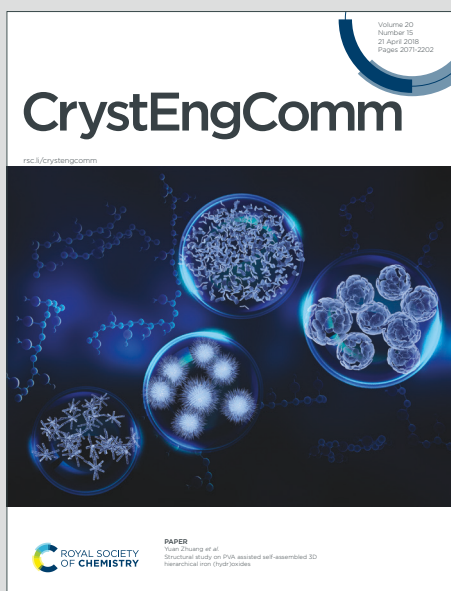


CrystEngComm

Accepted Manuscript

This article can be cited before page numbers have been issued, to do this please use: S. Kumar, S. Nandi, S. Suman and D. Halder, *CrystEngComm*, 2020, DOI: 10.1039/D0CE01199A.



This is an Accepted Manuscript, which has been through the Royal Society of Chemistry peer review process and has been accepted for publication.

Accepted Manuscripts are published online shortly after acceptance, before technical editing, formatting and proof reading. Using this free service, authors can make their results available to the community, in citable form, before we publish the edited article. We will replace this Accepted Manuscript with the edited and formatted Advance Article as soon as it is available.

You can find more information about Accepted Manuscripts in the [Information for Authors](#).

Please note that technical editing may introduce minor changes to the text and/or graphics, which may alter content. The journal's standard [Terms & Conditions](#) and the [Ethical guidelines](#) still apply. In no event shall the Royal Society of Chemistry be held responsible for any errors or omissions in this Accepted Manuscript or any consequences arising from the use of any information it contains.

A new dipeptide as selective gelator of Cu(II), Zn(II), Pb(II)†

Santosh Kumar,^a Sujay Kumar Nandi,^a Saurav Suman^a and Debasish Haldar^{*a}

Received 00th January 20xx,
Accepted 00th January 20xx

DOI: 10.1039/x0xx00000x

www.rsc.org/

The various aspects associated with the incorporation of steric constraints into a series of dipeptides have been studied. Self-assembly propensities of the dipeptides carried out with the use of complementary experimental methods enabled us to determine the effect of steric constraints. The Gly and Aib containing peptide **1** shows flakes-like morphology. Replacement of Gly by L-Phe in peptide **2** increase steric constraint and developed micro rods. Peptide **3** with N-phenyl glycine and L-Phe has a flower-like morphology, and peptide **4** with N-phenyl glycine and L-Tyr has microsphere morphology. The solid-state FT-IR studies show that the peptides are self-assembled by hydrogen bonds. From X-ray crystallography, peptide **1** adopts kink-like conformation and forms a supramolecular anti-parallel sheet-like structure through multiple intermolecular hydrogen bonds. Replacement of Gly by L-Phe helps the peptide **2** to adopt S-shape conformation and self-assembled to form a supramolecular helix in solid-state. Single crystal X-ray exhibits that the peptide **3** adopts extended conformation and form 2D sheet-like matrix through π - π stacking interactions. Moreover, metallogelation of peptide **3** was observed selectively for CuSO₄·5H₂O, ZnSO₄·7H₂O and Pb(OAc)₂·3H₂O, whereas other metals were not able to form gel. The study revealed a pivotal role played by the phenyl group in diverse self-assembly of the dipeptides.

Introduction

Molecular recognition and assembly and gelation is a spontaneous process which provides novel desired materials for eco-friendly biological applications.¹⁻⁴ Various compounds including block copolymers, surfactants, peptide derivatives, and lipid molecules have been adopted as building blocks for the development of supramolecular materials.⁵⁻⁷ Recently, small molecule containing aromatic groups have emerged as an appealing alternative for macromolecular systems to develop supramolecular materials due to their unique dynamic self-assembly propensities and stimuli responsiveness.⁸ So, the thorough understanding of chemical structures, physical properties, and self-assembly propensities of the building blocks are highly important.⁹⁻¹⁰ This self-assembly is mainly driven by various non-covalent interactions, including hydrogen bonding, π - π stacking, electrostatic interactions, and hydrophobic interactions.¹¹ Depending on the external environments, molecular structures and shapes, and relative volume fraction of hydrophilic and hydrophobic parts, these molecules self-assemble into diverse supramolecular

architectures, such as spherical or cylindrical micelles, vesicles, ribbons, and tubules.¹²⁻¹⁴ A number of supramolecular systems have been fabricated which can alter their topologies and properties upon exposure to external stimuli like solvents polarity, temperature, redox potential, light, sonication, and pH.¹⁵⁻¹⁷ Reches and Gazit fabricated nanofibers from self-assembly of diphenylalanine.¹⁸ Ulijn and co-workers have reported a hydrogel via π - π interlocked β -Sheets from the self-assemble dipeptide Phe-phe.¹⁹ Görbitz has reported the formation of nanoporous materials by self-assembly of amino acids and dipeptides.^{20,21}

We are developing peptide-based functional materials.²²⁻²⁵ Previously we have reported the diverse self-assembly and gas adsorption studies of isomeric hybrid peptides.²⁶ We have also developed a highly selective metallogel from 4-biphenylcarboxy capped diphenylalanine and FeCl₃.²⁷ Presently we have described topology-controlled selective Fe³⁺ binding in water by δ -peptides with dihydropyrimidinone containing amino acid.²⁸

In this regard, we have synthesized four boc- (**1** and **2**) and phenyl- (**3** and **4**) protected dipeptides by varying steric constraints. The solid-state structures show that the achiral dipeptide **1** adopts kink-like conformation and forms a supramolecular sheet-like structure through multiple intermolecular hydrogen bonds. But, the sterically hindered phenylalanine analogue dipeptide **2** shows S-shape conformation and forms a supramolecular helix. However, N-phenylglycine containing peptide **3** adopts extended

^a Department of Chemical Sciences

Indian Institute of Science Education and Research Kolkata
Mohanpur 741246, West Bengal, India

E-mail: deba_h76@iiserkol.ac.in, deba_h76@yahoo.com.

† Footnotes relating to the title and/or authors should appear here.

Electronic Supplementary Information (ESI) available: ¹H NMR, ¹³C NMR, solid state FTIR spectra, Figures ESI S1-2, Figure S3-S18, CCDC 2006561, 2006514 and 2006562. See DOI: 10.1039/x0xx00000x

conformation and forms a supramolecular 2D matrix through non-covalent interactions. From FESEM, depending on the steric constraints, the peptides show flakes, nanorods, flower, and microspheres morphology. Under basic condition, metallogelation of only peptide **3** was observed selectively for $\text{CuSO}_4 \cdot 5\text{H}_2\text{O}$, $\text{ZnSO}_4 \cdot 7\text{H}_2\text{O}$ and $\text{Pb}(\text{OAc})_2 \cdot 3\text{H}_2\text{O}$, whereas other metals were not able to form gel.

Experimental

Materials and reagents

All amino acid methyl esters and chemicals were purchased from Sigma chemicals.

Synthesis of Boc-Gly-Aib-OMe 1

1.75g (10 mmol) of Boc-Gly-OH was dissolved in 20 mL dry DCM in an ice-water bath. Aib-OMe was isolated from 1.95g (15 mmol) of the corresponding methyl ester hydrochloride by neutralization and subsequent extraction with ethyl acetate, and ethyl acetate extract was concentrated to 10 mL. It was then added to the reaction mixture, followed immediately by 2.53g (15 mmol) dicyclohexylcarbodiimide (DCC) and 2.30g (15 mmol) of hydroxybenzotriazole (HOBt). The reaction mixture was allowed to come to room temperature and stirred for 48 hrs. DCM was evaporated, and the residue was dissolved in ethyl acetate (60 mL), and dicyclohexylurea (DCU) was filtered off. The organic layer was washed with 2 M HCl (3 × 50 mL), brine (2 × 50 mL), 1M sodium carbonate (3 × 50 mL), and brine (2 × 50 mL) dried over anhydrous sodium sulphate; and evaporated in a vacuum to yield compound Boc-Gly-Aib-OMe as a solid. The product was purified by silica gel (100-200 mesh) using hexane-ethyl acetate as eluent. Yield: 2.45g (9.0 mmol, 90 %).

$^1\text{H-NMR}$ (400 MHz, CDCl_3 , δ ppm): 6.65 [b, 1H, amide NH], 5.39 [b, 1H, amide NH], 4.13 [dd, 2H, Gly- CH_2], 3.63 [s, 3H, OCH_3], 1.54 [s, 6H, Aib], 1.33 [s, 9H, Boc]. $^{13}\text{C-NMR}$ (100 MHz, CDCl_3 , δ ppm): 171.25, 165.71, 153.16, 77.38, 53.32, 49.50, 41.30, 25.15, 25.21, 21.16. Anal. Calcd for $\text{C}_{12}\text{H}_{22}\text{N}_2\text{O}_5$ (274): C, 52.54; H, 8.08; N, 10.21. Found: C, 52.57; H, 8.06; N, 10.18. Mass spectra, found m/z : 297.1509 [M+Na]⁺, calculated for $\text{C}_{12}\text{H}_{22}\text{N}_2\text{O}_5\text{Na}$ 297.1421.

Synthesis of Boc-Phe-Aib-OMe 2.

Boc-Phe-OH (1.75 g, 7 mmol) was dissolved in 50 mL dry DCM in an ice-cold water bath. $\text{H}_2\text{N-Aib-OMe}$ (1.2 g, 10 mmol) was dissolved in 10 mL DCM. It was then added to the reaction mixture, followed by immediate addition of 1.44 g (7 mmol) dicyclohexyl carbodiimide (DCC) and 0.95 g (7 mmol) of HOBt. The reaction mixture was allowed to come to room temperature and stir for 48 hrs. After that, DCM was evaporated, and the residue was dissolved in ethyl acetate (60 mL), and dicyclohexylurea (DCU) was filtered off. The organic layer was washed with 2 (M) HCl (3 × 50 mL), brine (2 × 50 mL), 1(M) sodium carbonate (3 × 50 mL) and brine (2 × 50 mL) and dried over anhydrous sodium sulfate. The solution was evaporated under vacuum to obtain dipeptide as a white solid. The product was purified by column chromatography. Yield: 1.96g (5.6 mmol, 80 %).

$^1\text{H-NMR}$ (500MHz, CDCl_3 , δ in ppm, 298 K): 7.26-7.27 (m, 2H, aromatic protons), 7.21-7.22 (m, 2H, aromatic protons), 7.22-7.20 (m, 1H, aromatic proton) 6.48 (s, 1H, Aib NH), 5.22-5.19 (s, 1H, Phe NH), 4.22 (m, 1H, Phe C^α H), 3.70 (s, 3H, OCH_3), 2.95-2.90 (m, 2H, Phe C^β H), 1.44 (s, 6H, Aib C^α H), 1.41 (s, 9H, BOC CH_3). $^{13}\text{C-NMR}$ (125 MHz, CDCl_3 , δ in ppm, 298 K): 174.17, 170.44, 156.31, 136.86, 129.54, 128.26, 126.95, 80.20, 56.43, 56.40, 52.65, 38.54, 28.32, 24.76; Anal. Calcd for $\text{C}_{19}\text{H}_{28}\text{N}_2\text{O}_5$ (364): C, 62.62; H, 7.74; N, 7.69. Found: C, 62.59; H, 7.76; N, 7.67. Mass spectra, found m/z : 387.4912 [M+Na]⁺, calculated for $\text{C}_{19}\text{H}_{28}\text{N}_2\text{O}_5\text{Na}$ 387.4824.

Synthesis of N-PhenylGly-Phe-OMe 3

N-phenylglycine-OH (1.51 g, 10 mmol) was dissolved in 50 mL dry DCM in an ice-cold water bath. $\text{H}_2\text{N-Phe-OMe}$ 1.81 g, 11 mmol) was dissolved in 10 mL DCM. It was then added to the reaction mixture, followed by immediate addition of 2.26 g (11 mmol) dicyclohexylcarbodiimide (DCC) and 1.48 g (11 mmol) of HOBt. The reaction mixture was allowed to come to room temperature and stir for 48 hrs. After that, DCM was evaporated, and the residue was dissolved in ethyl acetate (60 mL), and dicyclohexylurea (DCU) was filtered off. The organic layer was washed with 2 (M) HCl (3 × 50 mL), brine (2 × 50 mL), 1(M) sodium carbonate (3 × 50 mL) and brine (2 × 50 mL) and dried over anhydrous sodium sulfate. The products were purified by column chromatography using silica (60-120-mesh size) gel as stationary phase and n-hexane-ethyl acetate mixture as eluent. Yield: 2.05 g (6.5 mmol, 65 %).

$^1\text{H-NMR}$ (400 MHz, CDCl_3 , δ ppm): 7.23-7.14 [5H aromatic & 1H NH proton], 7.16-7.15[b,1H NH proton] 6.93-6.91[2H aromatic], 6.83[1H aromatic], 6.57-6.53[2H aromatic], 4.95-4.93 [m, C^βH], 3.77-3.75 [b, 2H], 3.69 [s, 3H, OCH_3], 3.06-3.05 [t, C^α 2H]. $^{13}\text{C-NMR}$ (100 MHz, CDCl_3 , δ ppm): 172.03, 170.68, 147.81, 129.74, 129.48, 128.91, 127.40, 119.50, 113.61, 52.87, 52.76, 48.95, 38.23. FT-IR (cm^{-1}): 3350, 2932, 1670, 1495. Anal. Calcd for $\text{C}_{18}\text{H}_{20}\text{N}_2\text{O}_3$ (312): C, 69.21; H, 6.45; N, 8.97. Found: C, 69.48; H, 6.42; N, 8.94. Mass spectra, found m/z : 335.1495 [M+Na]⁺, calculated for $\text{C}_{18}\text{H}_{20}\text{N}_2\text{O}_3\text{Na}$ 335.1407.

Synthesis of N-PhenylGly-Tyr-OMe 4

N-phenylglycine-OH (1.51 g, 10 mmol) was dissolved in 50 mL dry DCM in an ice-cold water bath. $\text{H}_2\text{N-Tyr-OMe}$ (2.14 g, 11 mmol) was dissolved in 10 mL DCM. It was then added to the reaction mixture, followed by immediate addition of 2.26 g (11 mmol) dicyclohexyl carbodiimide (DCC) and 1.48 g (11 mmol) of HOBt. The reaction mixture was allowed to come to room temperature and stir for 48 hrs. After that, DCM was evaporated, and the residue was dissolved in ethyl acetate (60 mL), and dicyclohexylurea (DCU) was filtered off. The organic layer was washed with 2 (M) HCl (3 × 50 mL), brine (2 × 50 mL), 1(M) sodium carbonate (3 × 50 mL) and brine (2 × 50 mL) and dried over anhydrous sodium sulfate. The products were purified by column chromatography using silica (60-120-mesh size) gel as stationary phase and n-hexane-ethyl acetate mixture as eluent. Yield: 2.23 g (6.7 mmol, 67 %).

$^1\text{H-NMR}$ (400MHz, CDCl_3 , δ ppm): 7.22-7.12[m,3H (aromatic)], 6.84-6.80[t, 1H aromatic], 6.76-6.74[d,2H aromatic], 6.59-6.57[d,2H

aromatic], 6.54-6.52[d, 2H aromatic], 6.4-6.3[b, 1H NH proton] 4.93-4.91[m, 1H], 4.24-4.15[b, 1H], 3.74-3.73[b, 2H, $^{\alpha}\text{CH}_2$ NPG], 3.71[s, 3H, OMe], 2.99-2.97[t, 2H, $^{\alpha}\text{CH}$ Tyr] ^{13}C -NMR (100 MHz, CDCl_3 , δ ppm): 172.32, 171.12, 155.57, 147.14, 130.59, 129.75, 127.21, 119.53, 115.90, 113.61, 53.01, 52.77, 48.88, 37.47. FT-IR (cm^{-1}): 3400, 2930, 1670, 1500. Anal. Calcd for $\text{C}_{18}\text{H}_{20}\text{N}_2\text{O}_4$ (328): C, 65.84; H, 6.14; N, 8.53. Found: C, 65.83; H, 6.17; N, 8.51. Mass spectra, found m/z : 351.1856 $[\text{M}+\text{Na}]^+$, calculated for $\text{C}_{18}\text{H}_{20}\text{N}_2\text{O}_4\text{Na}$ 351.1768.

NMR Experiments

All NMR experiments were performed on a Jeol 400 MHz and Bruker 500 MHz, spectrometer at 278 K. Compound concentrations were in the range 1–10 mM in CDCl_3 .

FT-IR Spectroscopy

Solid-state FT-IR spectra following KBr disk technique were measured in a Perkin Elmer Spectrum RX1 spectrophotometer.

Mass spectrometry

Mass spectra of the compounds were recorded on a Q-ToF Micro YA263 high-resolution (Waters Corporation) mass spectrometer by positive-mode electrospray ionization.

UV/Vis spectroscopy

The absorption spectra of the samples were recorded on a Perkin Elmer UV-Vis spectrophotometer.

Fluorescence spectroscopy

All fluorescence spectra were recorded on a Perkin Elmer fluorescent spectrometer (LS 55) using 1 cm path length quartz cell. Slit widths 2.5/2.5 were used.

Polarised Optical Microscope

A small amount of solution of the compound was placed on a clean glass coverslip and then dried by slow evaporation, then visualized at 40 \times magnification (Olympus optical microscope equipped with polarizer and CCD camera).

Single crystal X-ray diffraction study

Single crystal X-ray analysis of compounds **1-3** was recorded on a Bruker high-resolution X-ray diffractometer instruments with $\text{MoK}\alpha$ radiation. Data were processed using the Bruker SAINT package and the structure solution and refinement procedures were performed using SHELX97. CCDC 2006561, 2006514 and 2006562 contains the crystallographic data for the compounds **1-3** respectively.

Field Emission Scanning Electron Microscopy

Morphologies of the reported compounds were investigated using field emission-scanning electron microscopy (FE-SEM). For FE-SEM, a small amount of peptide solution or gel was drop casted on a clean glass coverslip and dried by slow evaporation at room temperature. Finally, the sample was dried under reduced pressure for two days at 30 $^{\circ}\text{C}$. The samples were gold-coated, and the micrographs were captured in Zeiss DSM 950 scanning electron microscope.

Transmission Electron Microscopy

Microstructure of the reported metallogels were investigated using transmission electron microscopy (TEM). For TEM, a small amount of gel was placed on a carbon coated copper grid and dried under vacuum for two days at 30 $^{\circ}\text{C}$. The micrographs were captured in JEOL JEM 2010 electron microscope.

Results and discussion

View Article Online

DOI: 10.1039/D0CE01199A

We have designed and synthesized four peptides with glycine, α -aminoisobutyric acid, L-phenylalanine, N-phenylglycine, and L-tyrosine to investigate the effect of increasing steric constraints. The achiral Boc-Gly-Aib-OMe **1** is less hindered than Boc-Phe-Aib-OMe **2**, N-PhenylGly-Phe-OMe **3**, and N-PhenylGly-Tyr-OMe **4** (Fig. 1). The assumption was that the steric constraints will restrict conformational flexibility and intervene on peptide folding and self-assembly. N-phenylglycine will enhance π - π stacking interaction and tyrosine was incorporated to include additional hydrogen bonding functionality. The main aim of this investigation was to control the structure and self-assembly of dipeptides by incorporating various steric constraints. Targeted dipeptides **1**, **2**, **3**, and **4** were synthesized by conventional solution-phase methodology using DCC/HOBT as coupling reagents. The final compounds have been purified by column chromatography and characterized by ^1H -NMR, ^{13}C -NMR, FT-IR and mass spectrometry (MS) analysis.

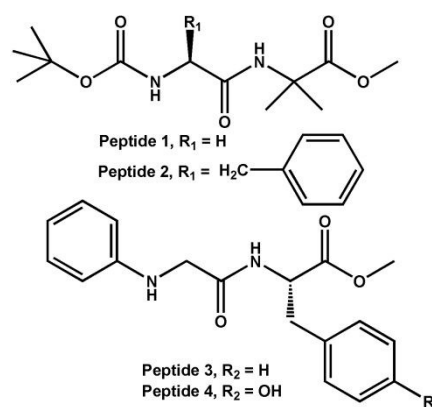


Fig. 1. The schematic presentation of dipeptides **1**, **2**, **3** and **4**.

To investigate the self-assembly behaviour of the dipeptides, a wide variety of different spectroscopic techniques have been used. The lack of a chromophore restricts peptide **1** for absorption and emission spectroscopy. Peptide **2** shows an absorption band at 259 nm, responsible for π to π^* transition, which does not shift with increasing concentrations (ESI Fig. S1a). We have also plotted the key absorbance intensities as a function of concentration of peptide **2** which shows the Beer-Lambert behavior is observed (ESI Fig. S2a). Peptide **2** shows emission peaks at 303 nm, which induces increasing intensity with increasing concentration (Fig. 2a). The typical UV-Vis absorption spectra of peptide **3** in methanol (1.0 μM) show absorption band at 241 nm and 288 nm for n to π^* and π to π^* transition (ESI Fig. S1b). However, increasing the concentration of **3** induces increasing intensity. The typical emission spectra of peptide **3** in methanol (1.0 μM), excitation done at 288 nm is shown in Fig. 2b. With increasing the concentration of peptide **3**, the emission band at 323 nm shows a bathochromic shift of 10 nm. For peptide **4**, absorption bands appear at 228 nm and 280 nm, responsible for n to π^* and π to π^* transition, which does not shift with increasing concentrations (Fig. 2c).

The plot of the key absorbance intensities as a function of concentration of peptide **4** exhibits the Beer-Lambert behavior (ESI Fig. S2c). The emission spectra of peptide **4** in methanol also show a band at 325 nm and a bathochromic shift of 14 nm with increasing concentration (Fig. 2d). These results show that the peptides **3** and **4** have similar aggregation pattern.

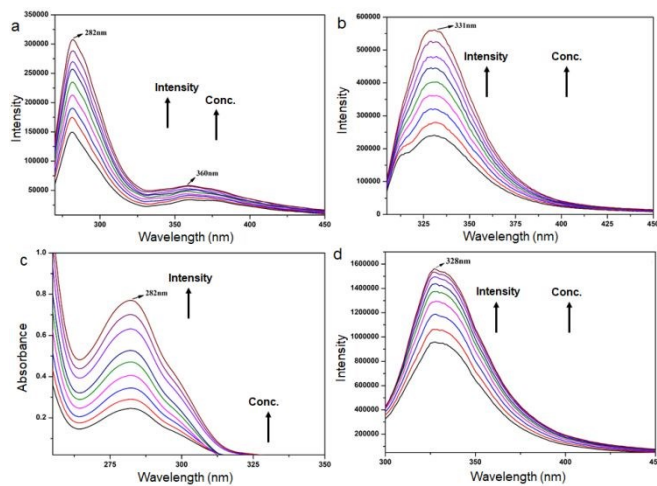


Fig. 2 (a) The emission spectra of peptide **2** in MeOH at 298 K with increasing concentrations (10 to 18 μM). Excitation done at 259 nm (b) The emission spectra of peptide **3** in MeOH at 298 K with increasing concentrations (10 to 18 μM). Excitation done at 288 nm. (c) The absorption spectra of peptide **4** in MeOH at 298 K with increasing concentrations (10 to 18 μM). (d) The emission spectra of peptide **4** in MeOH at 298 K with increasing concentrations (10 to 18 μM). Excitation at 280 nm.

Boc- and phenyl-protected peptides are soluble in organic solvents, but failed to form gel and exhibit morphological diversities. From field emission scanning electron microscopy (FE-SEM), the Boc protected achiral peptide **1** exhibits flake-like morphology (Fig. 3a). The Phe containing peptide **2** exhibits nano rod like morphology. The rods are unbranched. The diameter of the rods is c.a. 200 nm and several μm long. Moreover, the nano rods are assembled in a flower like structure. From FE-SEM, peptide **3** containing N-phenylglycine exhibits flower-like shape (Fig. 3c). However, the peptide **4** shows polydisperse microspheres morphology (Fig. 3d).

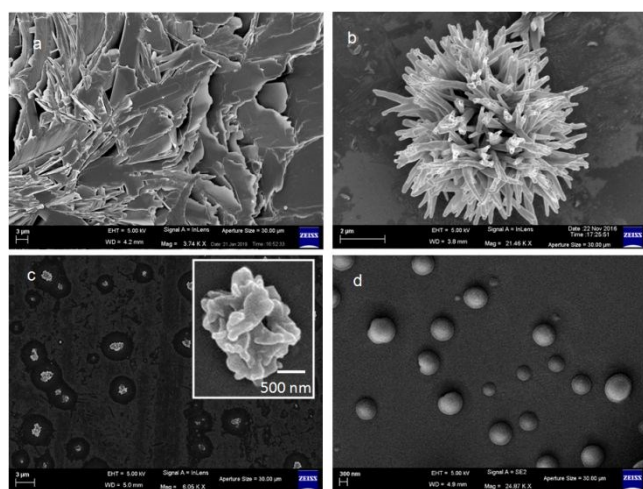


Fig. 3. FESEM images of (a) peptide **1** showing flakes-like morphology; (b) peptide **2** showing nanorods-like morphology, (c) peptide **3** having flower-like shape and (d) peptide **4** showing polydisperse microspheres morphology. The samples were prepared by drop casting the MeOH solution of the peptides on glass cover slip followed by drying at room temperature.

Solid state FT-IR spectroscopy is an excellent method to investigate the self-assembly propensity of the reported dipeptides. In FT-IR, the region of $3500\text{--}3200\text{ cm}^{-1}$ is important for the N-H stretching vibrations however the range $1800\text{--}1500\text{ cm}^{-1}$ is assigned for the stretching band of amide I and the bending peak of amide II.²⁹ For peptide **1**, Solid state FT-IR bands at 3314 cm^{-1} is responsible for hydrogen bonded NH's (Fig. 4a). The amide I and amide II bands appeared at 1670 and 1512 cm^{-1} . Peptide **2** show an intense band at 3373 and 3314 cm^{-1} indicating the NH groups are hydrogen bonded (Fig. 4b). The amide I and amide II bands have appeared at 1683 and 1539 cm^{-1} (Fig. 4b). The band at 1728 cm^{-1} is responsible for the ester C=O. The FT-IR spectra of peptide **3** exhibits NH stretching frequency at 3350 cm^{-1} for N-H and amide peaks at 1670 and 1495 cm^{-1} indicating the presence of extended Hydrogen bonded structures (Fig. 4c). For peptides **4**, the band at $3340\text{--}3400\text{ cm}^{-1}$ indicates that NH groups are non-hydrogen bonded and broadening due to OH stretching (Fig. 4d). The amide I and amide II bands have appeared at 1670 , 1590 and 1500 cm^{-1} respectively indicating the presence of extended H-bonded structures.²⁹ This suggests that the peptides **3** and **4** have significantly close conformations.

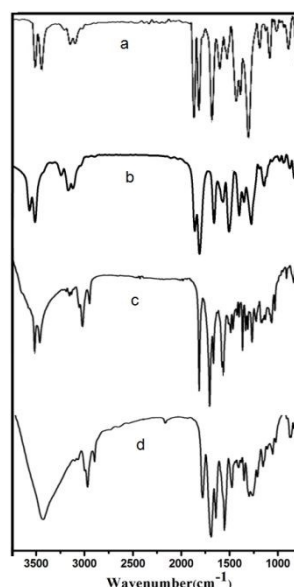


Fig. 4. The solid state FTIR spectra of (a) peptide **1**, (b) peptide **2**, (c) peptide **3**, (d) peptide **4**.

The molecular packing and solid-state self-assembly of the reported peptides **1**, **2**, and **3** at the atomic level were explained by X-ray crystallography.³⁰ We have failed to develop an X-ray quality crystal of peptide **4**. Crystals of peptides **1**, **2**, and **3** suitable for X-ray crystallography were obtained from methanol solution by slow evaporation. The peptide Boc-Gly-Aib-OMe **1** has one molecule in the asymmetric unit. The peptide **1** adopts a kink-like conformation (Fig. 5a). The selected backbone torsion angles are listed in Table 1. There is no intramolecular hydrogen bond. In higher-order packing, the individual subunits of peptide **1** are themselves regularly interlinked through hydrogen-bonding interactions, and thereby form an anti-parallel duplex structure (Fig. 5b). The duplex is further self-

assemble through multiple intermolecular hydrogen-bonding interactions to form supramolecular sheet-like structure along the crystallographic *b* direction (Fig. 5c). Hydrogen bonding parameters for peptide **1** are also listed in Table 2.

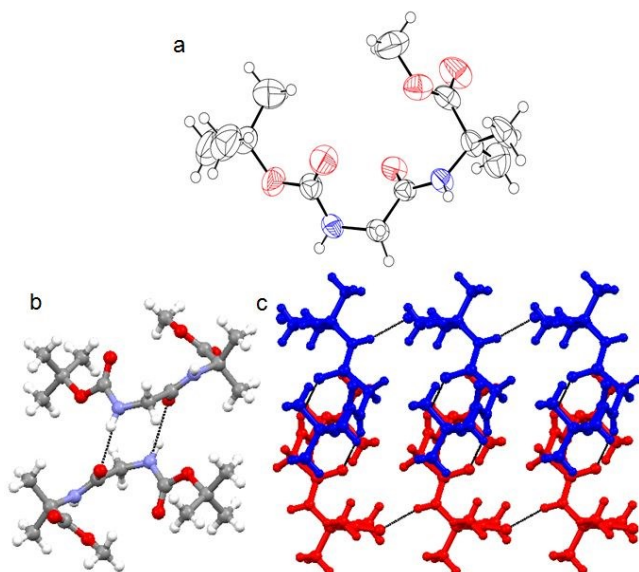


Fig. 5. (a) The ORTEP diagram of peptide Boc-Gly-Aib-OMe **1**. 50% probability level. (b) Ball and stick model of the hydrogen-bonded anti parallel duplex of peptide **1**. Intermolecular hydrogen bonds are shown as black dotted lines. (c) The supramolecular sheet-like structure of peptide Boc-Gly-Aib-OMe **1**. Hydrogen bonds are shown as black dotted lines.

The peptide **2** crystallizes with one molecule in the asymmetric unit (Fig. 6a). The peptide **2** adopts S-shape conformation (Fig. 6a), though there is no intramolecular hydrogen bond. The Boc amide group is in cis geometry (Fig. 6a). The selected backbone torsion angles are listed in Table 1. Further, the peptide **2** molecules form a supramolecular helix-like structure through multiple intermolecular hydrogen bonds (Fig. 6b) along the crystallographic *b* direction. The phenyl rings are outside of the supramolecular helical column (Fig. 6c). At higher-order assembly, supramolecular helical bundles stabilized by face to edge (T-shape) π - π stacking interactions (shortest centroid-C distance 3.8 Å) (Fig. 6d). The hydrogen bonding parameters are listed in Table 2.

From X-ray crystallography, it is evident that the asymmetric unit contains one molecule of peptide **3**. The crystal structure (Fig 7a) of peptide **3** shows that the peptide backbone adopts kink-like conformation stabilized by an intramolecular five-member N-H...N hydrogen bond. For peptide **3** molecule, face to face intramolecular π - π stacking interaction between Phe side chain and N-phenylglycine aromatic ring (centroid to centroid distance 4.3 Å) resulting in a rigid kink-like conformation in the solid-state (Fig 7a). The important backbone torsion angles are listed in Table 1. Hydrogen bonding parameters are listed in Table 2. The individual subunits of peptide **3** are themselves regularly interlinked through intermolecular hydrogen-bonding interaction, N4-H4...O1, and thereby form a supramolecular column-like structure along the crystallographic *b* direction (Fig. 7b). The higher-order packing through cooperative multiple intermolecular π - π interactions (Fig. 7c) of peptide **3**

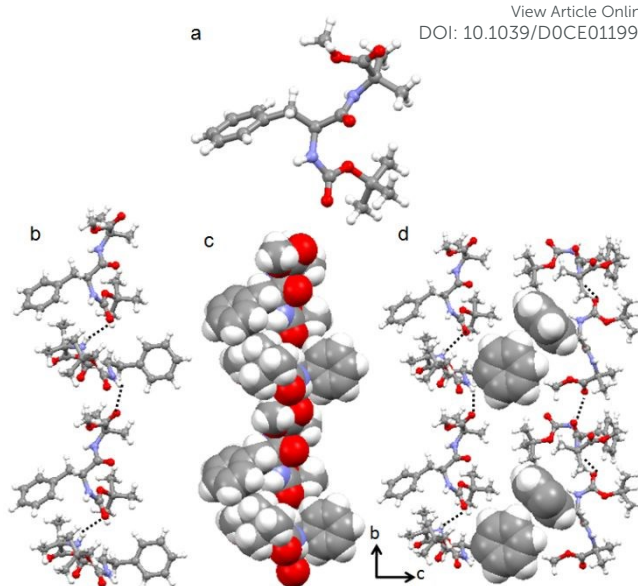


Fig. 6. (a) The solid-state conformations of peptide **2** molecules in the asymmetric unit. (b) The intermolecular hydrogen-bonded supramolecular helical assembly of peptide **2** in ball and stick model. Hydrogen bonds are shown as black dotted lines. (c) The supramolecular helical assembly of peptide **2** in space fill model. (d) The supramolecular helical bundle of peptide **2**, stabilized by T-shape π - π stacking interactions.

molecules shows a supramolecular 2D matrix-like structure (Fig. 7d) along crystallographic *a* and *c* direction. There are two intermolecular π - π interactions, face to face (shortest C-C distance 3.81 Å) and face to edge (shortest C-C distance 3.76 Å) (Fig. 7d).

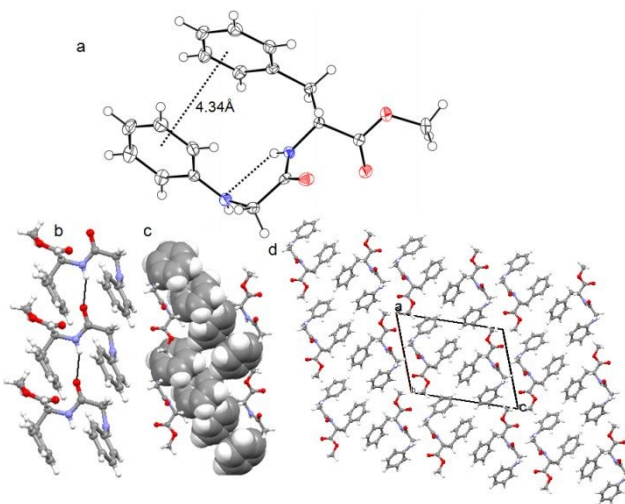


Fig. 7. (a) The ORTEP diagram of peptide **3**. 50% probability level. Intramolecular hydrogen bond and π - π stacking interactions are shown as black dotted lines. (b) Intermolecular hydrogen-bonded column-like structure of peptide **3**. Hydrogen bonds are shown as black dotted lines. (c) The multiple intermolecular π - π stacking interactions between peptide **3** molecules. (d) Supramolecular 2D matrix-like structure of peptide **3** by multiple intermolecular π - π interactions along crystallographic *a* and *c* direction.

Table 1. Selected backbone torsion angles (deg) for peptides **1**, **2** and **3**.

	$\phi_1/^\circ$	$\psi_1/^\circ$	$\phi_2/^\circ$	$\psi_2/^\circ$
Peptide 1	-60.7(2)	155.14(16)	48.4(2)	43.7(2)
Peptide 2	-64.5(7)	145.3(5)	-55.8(6)	-29.8(6)
Peptide 3	85.2(2)	12.0(2)	-74.7(2)	167.50(19)

Table 2. Hydrogen bonding parameters of peptides **1**, **2** and **3**^a

	D-H...A	D..H(Å)	H..A(Å)	D..A(Å)	D-H..A (°)
1	N2-H2...O4 ^a	0.86	2.07	2.9074(18)	163
	N1-H1...O3 ^b	0.86	2.12	2.9035(19)	152
2	N1-H1...O4 ^c	0.86	2.36	3.016(9)	133
	N2-H2...O2 ^d	0.86	2.21	2.954(9)	145
3	N2-H2...O1 ^e	0.86	2.47	3.213(3)	145

^aSymmetry equivalent $a = x, 1+y, z$, $b = -x, 1-y, 1-z$, $c = -x, -1/2+y, 3/2-z$, $d = 1-x, 1/2+y, 3/2-z$, $e = x, 1+y, z$.

Initially, the gelation abilities of the reported Boc- and phenyl-protected peptides were checked in various solvents by dissolving 10 mg of peptide in 1 mL of different solvents. Control experiments show that the Boc- and phenyl-protected peptides do not form a gel in any solvent by heating-cooling technique or even after sonication. However, the combination of peptide **3** with CuSO₄·5H₂O (1 equiv.) and NaOH (1.5 equiv.) exhibited the formation of black opaque gels. Typically, a weighted amount of peptide and an appropriate amount of a metal salt stock solution were placed into a screw-capped glass vial (4 cm length × 1 cm diameter). The mixture was stirred and sonicated for ~2 min until everything was homogeneous. The resulting solution was rest at room temperature. Among four peptides, only peptide **3** forms black opaque metallogel with CuSO₄·5H₂O (Fig. 8a). The minimum gelation concentration for peptide **3** is 12 mg/mL. The gel did not exhibit gravitational flow upon turning the vial upside-down at room temperature (Fig. 8a). We have also tried other metal ions. The peptide **3** with ZnSO₄·7H₂O (1 equiv.) and NaOH (1.5 equiv.) formed white opaque gels (Fig. 8b). The minimum gelation concentration for peptide **3** is 10 mg/mL. Similarly the peptide **3** in presence of Pb(OAc)₂·3H₂O (1 equiv.) and NaOH (1.5 equiv.) formed dirty white opaque gels (Fig. 8c). The minimum gelation concentration for peptide **3** is 12 mg/mL. Further peptide **3** was tested with other metal salts such as Cr, Ni, Hg, cd, Mg, Mn, and Pd sulfates and chloride complexes but all of them fail to form gel under same conditions. Fig. 8d shows that the peptide **3** fails to form gel with FeCl₃.

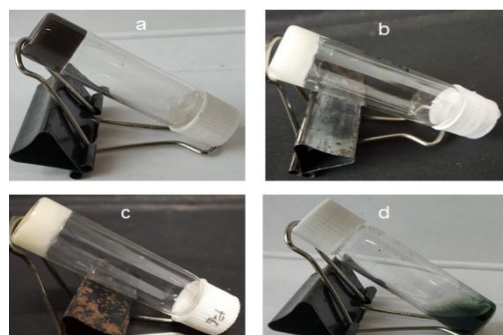


Fig. 8. (a) The black opaque gel of peptides **3** in presence of CuSO₄·5H₂O (1 equiv.) and NaOH (1.5 equiv.). (b) The white opaque gel of peptides **3** in presence of ZnSO₄·7H₂O (1 equiv.) and NaOH (1.5 equiv.). (c) The dirty white opaque gel of peptides **3** in presence of Pb(OAc)₂·3H₂O (1 equiv.) and NaOH (1.5 equiv.). (d) Peptide **3** failed to form gel in presence of FeCl₃ (1 equiv.) and NaOH (1.5 equiv.).

With increasing gelator concentration, the metallogel changes from soft gel to robust gel. This was further studied by gel melting experiments. Figure 9a shows the plots for change of gel–sol transition temperature (T_{gel}) of the peptide **3** in presence of CuSO₄·5H₂O and NaOH with increasing concentration. Change of gel–sol transition (T_{gel}) of the peptide **3** in ZnSO₄·7H₂O (1 equiv.) and NaOH (1.5 equiv.) with increasing gelator concentration is depicted in Fig. 9b. Gel to sol transition temperature (T_{gel}) of the peptide **3** in presence of Pb(OAc)₂·3H₂O (1 equiv.) and NaOH (1.5 equiv.) is 55.6 °C.

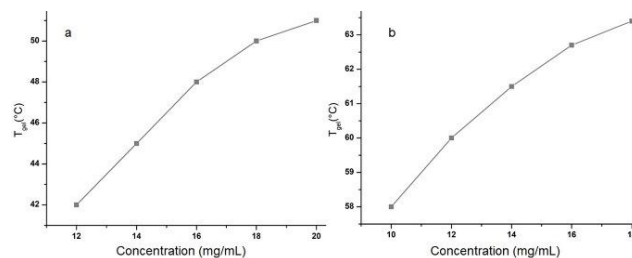


Fig. 9. (a) Change of gel–sol transition temperature (T_{gel}) of the peptide **3** in presence of CuSO₄·5H₂O and NaOH with increasing concentration. (b) Change of gel–sol transition temperature (T_{gel}) of the peptide **3** in presence of ZnSO₄·7H₂O and NaOH with increasing concentration.

The morphology of the metallogels were investigated by the field emission scanning electron microscopic studies (FE-SEM). The FE-SEM images of xerogel of peptide **3** and CuSO₄·5H₂O exhibit polydisperse fibrillar network structures (Fig. 10a,b). The average diameter of the fibrils is 10 nm and several μ m in length. Fig. 10c,d are showing the FE-SEM images of xerogel of peptide **3** and ZnSO₄·7H₂O. The xerogel has polydisperse fibril

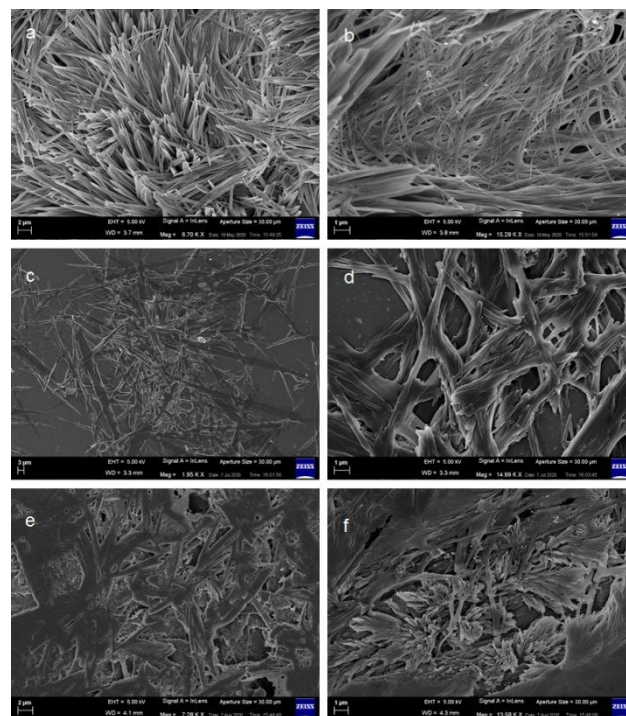


Fig. 10. FESEM images of (a) and (b) xerogel of peptide **3** and CuSO₄·5H₂O showing fibrillar network structures; (c) and (d) xerogel of peptide **3** and ZnSO₄·7H₂O showing polydisperse fibrils; (e) and (f) xerogel of peptide **3** and Pb(OAc)₂·3H₂O exhibiting highly entangled network morphology. FE-SEM has done with the dry metallogels (which was prepared in water) of peptide **3** placed on glass cover slip.

network structures. The average diameter of the fibrils is 500 nm and several μm in length. The FE-SEM images of xerogel of peptide **3** and $\text{Pb}(\text{OAc})_2 \cdot 3\text{H}_2\text{O}$ exhibit highly entangled network morphology (Fig. 10e,f). The average diameter of the fibrils is 100 nm and several μm in length.

To understand the microstructure of the metallogels, transmission electron microscopy (TEM) have performed. The TEM images of xerogel of peptide **3** and $\text{CuSO}_4 \cdot 5\text{H}_2\text{O}$ exhibit polydisperse fibril morphology (Fig. 11a,b). Fig. 11c shows the TEM image of xerogel of peptide **3** and $\text{ZnSO}_4 \cdot 7\text{H}_2\text{O}$. The xerogel has polydisperse fibrillar network structures. The TEM images of xerogel of peptide **3** with $\text{Pb}(\text{OAc})_2 \cdot 3\text{H}_2\text{O}$ exhibit entangled fibril morphology (Fig. 11d).

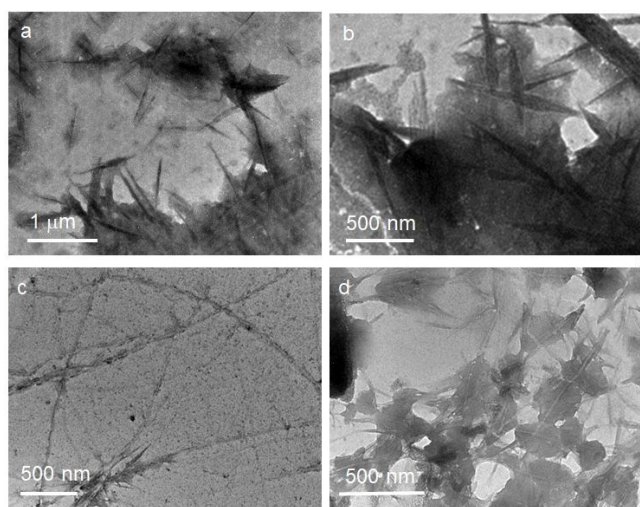


Fig. 11. TEM images of (a) and (b) xerogel of peptide **3** and $\text{CuSO}_4 \cdot 5\text{H}_2\text{O}$ showing polydisperse fibril morphology; (c) xerogel of peptide **3** and $\text{ZnSO}_4 \cdot 7\text{H}_2\text{O}$ showing fibrillar network structures; (d) xerogel of peptide **3** with $\text{Pb}(\text{OAc})_2 \cdot 3\text{H}_2\text{O}$ (1 equiv.) and NaOH (1.5 equiv.) exhibiting entangled fibril morphology.

Conclusions

In conclusion, we have synthesized four dipeptides by varying steric constraints, which exhibit diverse self-assembly. In solid-state, the peptide **1** forms anti-parallel dimer and supramolecular sheet-like structure in higher order. But, the hindered phenylalanine analogue shows a supramolecular helical structure through intermolecular hydrogen bonds and π - π stacking interactions. The N-phenylglycine containing peptide **3** adopts kink-like conformation and forms a supramolecular 2D matrix stabilized by multiple π - π stacking interactions. Moreover, The peptide **1** shows flakes-like morphology. Replacement of Gly by Phe (peptide **2**) developed micro rods. Peptide **3** with N-phenylglycine and L-Phe has flower-like morphology, and peptide **4** with N-phenylglycine and L-Tyr has microsphere morphology. Only peptide **3** forms metallogels selectively with $\text{CuSO}_4 \cdot 5\text{H}_2\text{O}$, $\text{ZnSO}_4 \cdot 7\text{H}_2\text{O}$ and $\text{Pb}(\text{OAc})_2 \cdot 3\text{H}_2\text{O}$. The information obtained may be helpful for the engineering of peptidic functional materials.

Conflicts of interest

There are no conflicts to declare.

Acknowledgements

This work was financed by IISER-Kolkata. S. Kumar and S. K. Nandi acknowledges the CSIR, India for research fellowship.

Notes and references

- 1 T. Shimizu, M. Masuda and H. Minamikawa, *Chem. Rev.*, 2005, **105**, 1401–1443.
- 2 N. L. Rosi and C. A. Mirkin, *Chem. Rev.*, 2005, **105**, 1547–1562.
- 3 Y.-b. Lim, K.-S. Moon and M. Lee, *Chem. Soc. Rev.*, 2009, **38**, 925–934.
- 4 S. Cavalli, F. Albericio and A. Kros, *Chem. Soc. Rev.*, 2010, **39**, 241–263.
- 5 T. Shimizu, R. Iwaura, M. Masuda, T. Hanada and K. Yase, *J. Am. Chem. Soc.*, 2001, **123**, 5947–5955.
- 6 J. T. Davis and G. P. Spada, *Chem. Soc. Rev.*, 2007, **36**, 296–313.
- 7 I. C. Reynhout, J. J. L. M. Cornelissen and R. J. M. Nolte, *Acc. Chem. Res.* 2009, **42**, 681–692.
- 8 S. S. Babu, V. K. Praveen and A. Ajayaghosh, *Chem. Rev.* 2014, **114**, 1973–2129.
- 9 E. Krieg, M. M. C. Bastings, P. Besenius and B. Rybtchinski, *Chem. Rev.*, 2016, **116**, 2414–2477.
- 10 X. Du, J. Zhou, J. Shi and B. Xu, *Chem. Rev.*, 2015, **115**, 13165–13307.
- 11 S. Hect and I. Huc, *Foldamers: Structure, Properties and Applications*, Wiley-VCH, Weinheim, 2007.
- 12 R. Klajn, J. F. Stoddart and B. A. Grzybowski, *Chem. Soc. Rev.*, 2010, **39**, 2203–2237.
- 13 A. Ajayaghosh and V. K. Praveen, *Acc. Chem. Res.*, 2007, **40**, 644–656.
- 14 A. C. Heras, S. Pennadam, C. Alexander, *Chem. Soc. Rev.*, 2005, **34**, 276–285.
- 15 P. M. Mendes, *Chem. Soc. Rev.*, 2008, **37**, 2512–2529.
- 16 S. Yagai and A. Kitamura, *Chem. Soc. Rev.*, 2008, **37**, 1520–1529.
- 17 S. I. Kawano, N. Fujita and S. Shinkai, *J. Am. Chem. Soc.*, 2004, **126**, 8592–8593.
- 18 (a) M. Reches and E. Gazit, *Science* 2003, **300**, 625–627; (b) M. Reches, E. Gazit, *Isr. J. Chem.*, 2005, **45**, 363–371.
- 19 A. M. Smith, R. J. Williams, C. Tang, P. Coppo, R. F. Collins, M. L. Turner, A. Saiani and R.V. Ulijn, *Adv. Mater.*, 2008, **20**, 37–41.
- 20 C. H. Görbitz, *Chem. Commun.*, 2006, 2332–2334.
- 21 C. H. Görbitz, *CrystEngComm.*, 2005, **7**, 670–673.
- 22 S. K. Maity, S. Maity, P. Jana and D. Haldar, *Chem. Commun.*, 2012, **48**, 711–713.
- 23 S. K. Maity, S. Bera, A. Paikar, A. Pramanik and D. Haldar, *Chem. Commun.*, 2013, **49**, 9051–9053.
- 24 P. Jana, A. Paikar, S. Bera, S. K. Maity and D. Haldar, *Org. Lett.*, 2014, **16**, 3841.
- 25 K. Maji, R. Sarkar, S. Bera and D. Haldar, *Chem. Commun.*, 2014, **50**, 12749–12752.
- 26 S. Maity, P. Jana, S. K. Maity, P. kumar and D. Haldar, *Crystal Growth and Design*, 2012, **12**, 422–428.
- 27 S. Sasmal, K. Maji, David Diaz Diaz and D. Haldar, *CrystEngComm.*, 2019, **21**, 4289–4297.
- 28 D. Podder, S. Sasmal, S. Konar, P. Ghorai and D. Haldar, *Crystal Growth & Design*, 2020, **20**, 1760–1770.

ARTICLE

Journal Name

- 29 (a) M. Toniolo, *Biopolymers* 1977, **16**, 219-224; (b) V. Moretto, M. Crisma, G. M. Bonora, C. Toniolo, H. Balaram and P. Balaram, *Macromolecules* 1989, **22**, 2939-2944.
- 30 Single crystal X-ray analysis of peptides **1-3** were recorded on a Bruker high resolution X-ray diffractometer instrument. The structures were solved by a direct method and refined by least-squares calculations on F2 for all independent reflections (SHELXL-2014). Crystal Data of peptide **1**: $C_{12}H_{22}N_2O_5$, Mw = 274.32, P 21/c, a = 11.6077(4) Å, b = 5.8948(2) Å, c = 23.3133(10) Å, $\alpha = 90^\circ$, $\beta = 100.550(4)^\circ$, $\gamma = 90^\circ$, V = 1568.25(10) Å³, Z = 4, T = 293 K, $D_{calc} = 1.162 \text{ g/cm}^3$, REM Flack = n/a, R1 = 0.0465 and wR2 = 0.1307. Crystal Data of peptide **2**: $C_{19}H_{28}N_2O_5$, Mw = 364.43, P 21 21 21, a = 8.279(17) Å, b = 11.90(3) Å, c = 20.37(4) Å, $\alpha = 90^\circ$, $\beta = 90^\circ$, $\gamma = 90^\circ$, V = 2007(8) Å³, Z = 4, T = 273 K, $D_{calc} = 1.206 \text{ g/cm}^3$, REM Flack = -1(3), R1 = 0.0586 and wR2 = 0.1460. Crystal Data of peptide **3**: $C_{18}H_{20}N_2O_3$, Mw = 312.36, P 21, a = 10.9817(6) Å, b = 5.3645(3) Å, c = 14.6541(9) Å, $\alpha = 90^\circ$, $\beta = 109.547(6)^\circ$, $\gamma = 90^\circ$, V = 813.54(9) Å³, Z = 2, T = 100 K, $D_{calc} = 1.275 \text{ g/cm}^3$, REM Flack = 0.1(3), R1 = 0.0374 and wR2 = 0.1027.. CCDC 2006561, 2006514 and 2006562 contains the crystallographic data for the compounds **1**, **2** and **3** respectively.

View Article Online
DOI: 10.1039/D0CE01199A

TOC Graphic

A new dipeptide as selective gelator of Cu(II), Zn(II) and Pb(II)Santosh Kumar,^a Sujay Kumar Nandi,^a Saurav Suman^a and Debasish Haldar^{*a}

Metallogelation was observed selectively for CuSO₄, ZnSO₄ and Pb(OAc)₂ and dipeptide containing N-phenylglycine and L-Phe, whereas other metals and analogues dipeptides were failed to form gel.

